Influence of engineered roughness microstructures on adhesion and turbulent resuspension of microparticles

Amir Banari, Klaus Graebe, Martin Rudolph, Ehsan Mohseni, Pierre Lorenz, Klaus Zimmer, René Hübner, Christophe Henry, Mireille Bossy, Uwe Hampel, et al.

Influence of engineered roughness microstructures on adhesion and turbulent resuspension of microparticles

Amir Banari,[1] Klaus Graebe,[2] Martin Rudolph,[2] Ehsan Mohseni,[1] Pierre Lorenz,[3] Klaus Zimmer,[3] René Hübner,[4] Christophe Henry,[5] Mireille Bossy,[5] Uwe Hampel,[1,6] Gregory Lecrivain[1,*]

[1] Helmholtz-Zentrum Dresden-Rossendorf, Institut für Fluiddynamik, Bautzner Landstraße 400, 01328 Dresden, Germany

[2] Helmholtz-Zentrum Dresden-Rossendorf, Helmholtz Institute Freiberg for Resource Technology, Chemnitzer Straße 40, 09599 Freiberg, Germany

[3] Leibniz-Institut für Oberflächenmodifizierung, Permoserstraße 15, 04318 Leipzig, Germany

[4] Helmholtz-Zentrum Dresden-Rossendorf, Institut für Ionenstrahlphysik und Materialforschung, Bautzner Landstr. 400, 01328 Dresden, Germany

[5] Université Côte d'Azur, Inria, CNRS, Cemef, France

[6] Technische Universität Dresden, Institut für Energietechnik, Professur für Bildgebende Messverfahren für die Energie- und Verfahrenstechnik, 01069 Dresden, Germany

[*] Corresponding author. E-Mail: g.lecrivain@hzdr.de, Tel: +49 351 260 – 3768

Abstract: From microplastics resuspending into the atmosphere to earth particles left behind during extraterrestrial explorations, the resuspension of microparticles by a turbulent gas flow occurs in many natural, environmental and industrial systems. Wall surfaces, onto which particles initially adhere, are rarely smooth and this surface roughness affects particle resuspension. Available experimental data on particle resuspension have been obtained with substrates, whose surfaces are either unaltered or manually abraded with, for instance, sand blasting. In these experiments, the roughness elements span a wide size range and are in-homogeneously distributed in space. Surface functionalization is a modern technique allowing the precise fabrication of a wall surface with well-characterized microstructures, hence reducing the asperity randomness associated with conventional abrasion techniques. Taking advantage of surface functionalization, we present here a new set of reference data, where the wall asperities are represented by a structured arrangement of micropillars and microcubes. Adhesion force measurements and particle remaining fraction against gas velocity, at Reynolds number up to 8000, are reported for one reference and two artificially roughened substrates. Laboratory measurements show that the microasperities have little to moderate effect on the mean adhesion force and the threshold velocity, at which half of the 100-µm particles resuspend. The standard deviations are, however, much more affected. The presented results will primarily contribute to the improvement of resuspension models, which until now rely on a simplified representation of the surface roughness elements. The presented measurements are highly compatible with such models, which involve elementary roughness features, such as hemispherical asperities superimposed with a flat plate.

Keywords: Particle resuspension, adhesion force measurement, turbulent gas flow, surface functionalization, surface roughness.

1. Introduction

1.1. General context

The detachment of micron particles from a wall surface by a turbulent gas flow, hereafter referred to as resuspension, is present in many natural and industrial environments. Examples are diverse and range from pathogens detaching from indoor and outdoor surfaces (Bourouiba, 2021; Hospodsky et al., 2012) to pollen (Banari, Hertel, Schlink, Hampel, & Lecrivain, 2023; Visez et al., 2019), microplastics (Amato-Lourenco et al., 2020), volcanic ash (Del Bello et al., 2018), soot (Cho et al., 2021), minerals in arid environments (Klose & Shao, 2013), radioactive dust (Gregory Lecrivain, Vitsas, Boudouvis, & Hampel, 2014; Shinohara & Yoshida-Ohuchi, 2021) and earth particles adversely transported during extraterrestrial explorations (Mikellides et al., 2020).

1.2. State-of-the-art and current limitations

In the simplest scenario, where an individual particle initially sits at rest on a wall surface, resuspension occurs when either the aerodynamic drag force or torque overcomes its adhesive counterpart (Henry & Minier, 2014a; Henry, Minier, & Brambilla, 2023). Wall surfaces are however rarely smooth and wall roughness significantly affects the adhesion force pinning the particle to the substrate (Brambilla & Brown, 2020). Many experiments performed with the ambient fluid at rest support the idea that an increased wall roughness results in a lower adhesion force. Early experiments were performed by vertically pulling rubber particles from a polymer PMMA wall surface (Fuller & Tabor, 1997). By increasing the wall roughness from about 0.1 to 1 µm, the authors reported a ten-fold reduction in the adhesion force. In their work, the wall roughness was achieved by bead-blasting the samples. Later, Atomic Force Microscopy (AFM) was used to precisely determine the pull-off force needed to detach glass spheres with a 20-µm diameter from a titanium wall surface (Rabinovich, Adler, Ata, Singh, & Moudgil, 2000). By increasing the surface wall roughness from 0.17 to 1.60 nm, the authors reported an almost four-fold reduction in the adhesion force. Similar conclusions were recently drawn for spherical tungsten particles with a 20-µm diameter pulled off a tungsten surface (Peillon et al., 2019). Compared to the nanometer range, it was found that a wall roughness in the micrometer range results in a decrease in the adhesion force by up to two orders of magnitude.

In addition to AFM measurements, a few experimental studies have investigated the role played by the substrate roughness on particle resuspension in a turbulent gas flow (Barth, Preuß, Müller, & Hampel, 2014; Brambilla, Speckart, & Brown, 2017; Brambilla, Speckart, Rush, Montano, & Brown, 2018; Goldasteh, Ahmadi, & Ferro, 2013; Jiang, Matsusaka, Masuda, & Qian, 2008; Mukai, Siegel, & Novoselac, 2009; Peillon et al., 2022). In the work by Jiang et al. (2008), spherical glass and PMMA particles with diameters ranging from about 10 to 40 µm were resuspended from stainless steel substrates. The wall roughness of the substrates ranged from 10 nm to 1.64 µm and was obtained by manual abrasion with sandpaper. It was showed that the greater the wall roughness, the smaller the threshold velocity ($u^*_{0.5}$), here defined as the friction velocity, at which 50 % of the particles resuspend. Conversely, this trend was not observed for the lighter PMMA particles when the wall roughness exceeded 0.3 µm, thereby not corroborating the fact that increased wall roughness triggers increased material detachment. One possible reason for this unexpected behavior is the increased near-wall turbulence generated by the larger wall roughness and the lower inertia of the PMMA particles. Further experimental studies on the determination of the threshold velocity with increasing wall

roughness have been done by Mukai et al. (2009). In their work, salt particles with sizes ranging from 1 to 20 µm were resuspended from linoleum and galvanized metal plates, whose surface roughness was estimated from literature data at 0.08 and 0.15 mm, respectively. With relatively high turbulence intensity, no significant difference in the threshold velocity was observed. In a later experiment (Barth et al., 2014), smooth glass plates with a wall roughness of 25 nm and abraded steel plates with a wall roughness set to 0.08, 0.92 and 1.54 µm were used. The diameter of the glass beads ranged from 25 to 45 µm. The authors could not report any correlation between wall roughness and threshold velocity.

To simulate particle resuspension, computationally tractable models have been suggested. In this context, many authors have described the wall roughness with simplified descriptions at the level of the particle size. One approach is to describe the rough surface of the substrate as a smooth plate covered with randomly placed hemispherical asperities (Cui & Sommerfeld, 2022; Guingo & Minier, 2008; Henry & Minier, 2014b; Rabinovich et al., 2000; Ziskind, Fichman, & Gutfinger, 1997). Such geometrical representations make it possible to conveniently estimate an adhesion force with a van der Waals formulation based on asperity and particle radii. Alternative representations of the roughness elements exist. Nasr, Ahmadi, Ferro, and Dhaniyala (2019), for instance, described the wall roughness with a two dimensional sinusoidal function and Hu, Johnson, and Meneveau (2023) with multi-fractal roughness elements. Simulations with the above adhesion models, which are often coupled to a force-balance model to simulate the rupture of the adhesive bond by aerodynamic forces, generally deliver matching threshold velocities for various roughness lengths. In addition, such simulations allow a detailed investigation of the triggering resuspension mechanisms, such as the particle rocking with an asperity (Brambilla et al., 2018; Guingo & Minier, 2008), that is otherwise difficult to observe experimentally. In some other studies (Soltani & Ahmadi, 1999), the roughness of the particle surface is also taken into account. While numerical simulations are out of the scope in this study, it is important to note that the validation of the existing models is often hampered by the lack of precise information on roughness characteristics, especially with respect to shape and curvature of the roughness elements as well as their exact spatial repartition on the substrate (Henry & Minier, 2018).

1.3. Objectives of this work

Following the brief overview of the above state-of-the-art, wall roughness appears to play a role in particle resuspension. Experiments on particle resuspension by turbulent gas flows have been carried out, in which the wall roughness of the substrates has been changed by mechanical abrasion, for instance with sandblasting or sandpaper. The reported results are somewhat controversial and do not always support the assumption, that an increased wall roughness causes particle resuspension to occur at a lower friction velocity. The wall roughness of real-life substrates is random in nature, with wall asperities highly inhomogeneous in space and size. This in-turn leads to an intricate interaction between wall and particle surfaces that continues to challenge the modeling, especially in terms of adhesion force formulations (Henry & Minier, 2018). Available resuspension models rely on an ideal description of the wall surface, which aims at being statistically representative of those used in experiments. Despite continuous efforts in terms of modeling, this ideal surface representation still fails to fully capture the chaotic and nonlinear nature of experimentally used rough surfaces. The objectives of this work are twofold:

- first, to determine experimentally the adhesion force between an individual spherical microparticle and a wall surface artificially roughened with a structured arrangement of identical and geometrically simple roughness elements,
- second, to link it with the resuspension of a particle cloud initially at rest on the same wall surface and exposed to a turbulent gas flow.

To the authors' knowledge, we provide here first experimental data obtained by using a structured arrangement of well-defined asperities as replacement to naturally arising asperities with uneven size distribution and random placement. Adhesion force measurements with an AFM and particle remaining fraction against gas velocity in a wind channel are here reported for a reference smooth surface (S1) and two artificially roughened surfaces (S2 and S3). The well-defined asperities in S2 and S3 are represented by cylindrical micropillars and microcubes.

The paper is organized as follows: the methods and experimental procedure are described in Section 2, while the results obtained are reported and analyzed in Section 3.

2. Methods

2.1. Scenarios

Three experimental scenarios are presently investigated. In the first reference scenario (S1) illustrated in Figure 1a, an individual spherical particle is initially at rest on an unaltered and aerodynamically smooth horizontal wall surface and is exposed to a turbulent gas flow. The arrow F_a pointing downwards represents the adhesion force. We hereafter define a "smooth" wall surface, as a surface with roughness features in the nanometer range. The first-order roughness is typically below 5 nm, that is a size by several orders of magnitude lower than the asperity height (h) set in the scenarios S2 and S3. In the second scenario (S2) illustrated in Figure 1b, the wall surface of the substrate is artificially roughened by well-defined microasperities arranged in a square lattice. Each asperity is a cylindrical micropillar with a diameter set to δx = 5 µm and a height h = 5 µm. The separation distance between two asperities is also δx. As shown later, the cross-sectional contour of a micropillar is not truly a circle but rather a square with rounded corners. In the third scenario (S3) illustrated in Figure 1c, the asperities are microcubes arranged in a two-dimensional face-centered layout reminiscent of a chessboard. The side length of each microcube is set to δx = 7.5 µm and the height to h = 5 µm. It is here postulated that the total adhesion force $\sum(F_a)_i$ originating from the rough surfaces S2 and S3 is lower than that from the reference substrate S1. Because the contact area between a single particle and the rough substrate is smaller, we anticipate that resuspension occurs at a lower gas velocity (U). Note that Figure 1 is purely illustrative and aims at describing our postulate. The softness of the glass particles, from which the adhesion forces can be established from theories of contact mechanics, for instance with the JKR or the DMT model (Ciavarella, Joe, Papangelo, & Barber, 2019), is deliberately exaggerated.

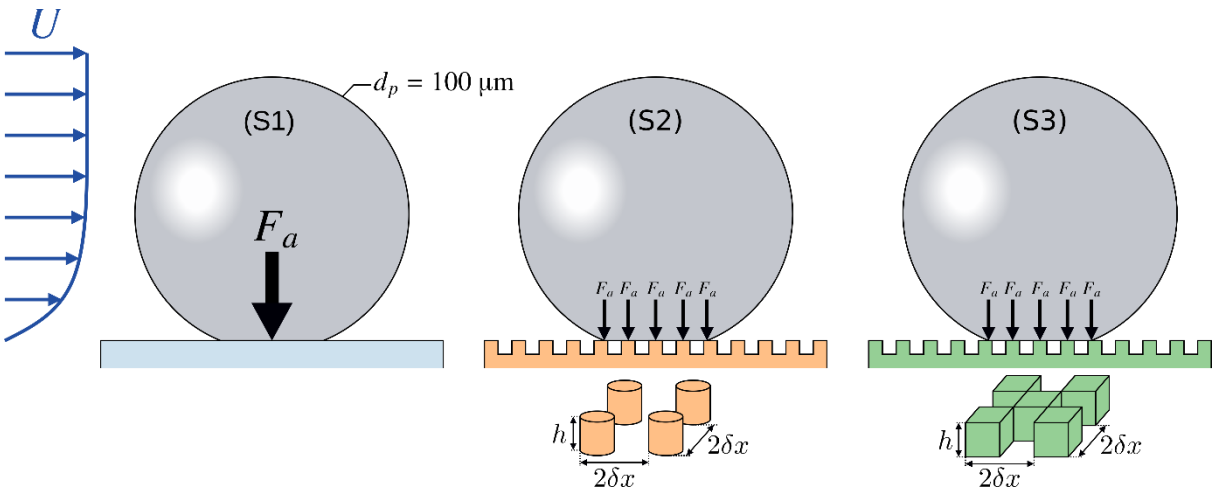

***Fig. 1**: Schematics of the presented experimental tests. In the reference scenario (S1), a spherical particle sits on a smooth surface. The adhesion force is F_a. In scenarios (S2) and (S3), the particle sits on a structured arrangement of microcubes and cylindrical micropillars. It is postulated, that in S2 and S3, the resulting adhesion force $\sum F_a$ is lower than the reference value in S1. For illustration purposes, the deformation of the particles, from which the adhesion forces can be established with theories of contact mechanics, has been exaggerated.*

2.2. Particles

The particle beads are here spherical and made of soda lime-silicate particles (GBL100, Association of Powder Process Industry and Engineering). They are highly monodispersed in size and have a density of ρ_p = 2,500 kg·m^{-3}. With a particle-to-air density ratio $\rho_p/\rho \approx 2000$, the particles are much heavier than the ambient gas. With a particle diameter set to d_p = 100 µm, the particles are classified as coarse to super coarse (Adebiyi et al., 2023). The particle size is, among others, representative of settling dust, pollen and ash particles (Del Bello et al., 2018; Klose & Shao, 2013; Visez et al., 2019). A further motivation behind this relatively large particle size was to have a ratio of the particle diameter to asperity height matching that reported in other experimental studies. It turned out a lot more practical to change the particle size rather than the asperity height. Here, the ratio equals d_p/h = 20. In the experiments performed by Barth et al. (2014) and Jiang et al. (2008), threshold velocities were obtained with a ratio of particle diameter to mean wall roughness equal to about 30.

2.3. Surface functionalization of the substrates

The three substrates presently used are wafers that are precision thin round windows (Product 226-1226E, EKSMA Optics, Lithuania). These have been functionalized with one smooth and two rough coatings. The coating procedure for the rough substrates is as follows. The substrate surface is first prepared with a standard two-step wafer cleaning process, known as RCA clean. The first cleaning step is performed with a NH3/H2O2/H2O solution at 50 – 60 °C in an ultrasonic bath for 20 min and the second with a HCl/H2O2/H2O solution at 50 – 60 °C, also in an ultrasonic bath for 20 min. The substrate is then covered with an adhesion promoter (TI Prime, Microchemicals) by spin-coating with a rotation speed of 4000 rpm and a subsequent drying at 115 °C for 2 min. The substrate surface is then covered with a negative photoresist (AR-N4400-10, Allresist) by spin-coating with 4000 rpm and a subsequent drying at 90°C for 4 min. The resulting photoresist layer exhibits a thickness of about 5 µm. Photolithographic exposure of the resist is performed with a mercury vapor lamp (3×5 s) using a chrome

lithography mask with a periodic grating. For the lithography mask in S2, squares with a 5 µm side length and a 10 µm periodicity in the two lattice directions are used. Owing to the lithography fabrication process, the asperities appear from the top view as squares with rounded corners. For the mask in S3, squares with both edge length and period set to 7,5 µm are used. The irradiated sample is tempered at 100 °C for 5 min and then developed by a developer (AR-300-47) for 75 s. Following the developing process, the sample is dried at 95 °C for 2 min and additionally flood-exposed with a mercury vapor lamp for 15 s. A final tempering process carried out at 120°C for 5 min is applied to improve the mechanical stability. With exception of the last steps, the procedure used to fabricate the smooth reference coating S1 is the same as described above, meaning that a 5-µm thin photoresist layer is present on the clean wafer surface. Based on previous works (Maji, Urakawa, & Inoue, 2014; Monk, Haskins, Bauschlicher, & Lawson, 2015), the Young's modulus of a typical Novolak resin (AR-N4400-10) normally ranges from 3 to 6 GPa and the Poisson's ratio from 0.3 to 0.36.

Top-down images of a glass particle at rest on the three substrates are shown in Figure 2. The micrographs were taken at different magnifications with a scanning electron microscope (SEM). The smoothness of the reference substrate surface and the asperities in S2 and S3 are well distinguishable. With respect to S1, the measured first-order roughness of the surface is within 5 nm, that is a size by several orders of magnitude lower than the asperity height (h) set in S2 and S3. Despite very few spots with damaged asperities that may have adversely occurred during fabrication and/or manipulation of the substrates during the measurement campaign, the quality of the coating is generally good. Further SEM images with a larger field of view can be seen in the raw data material (Gregory. Lecrivain, 2023).

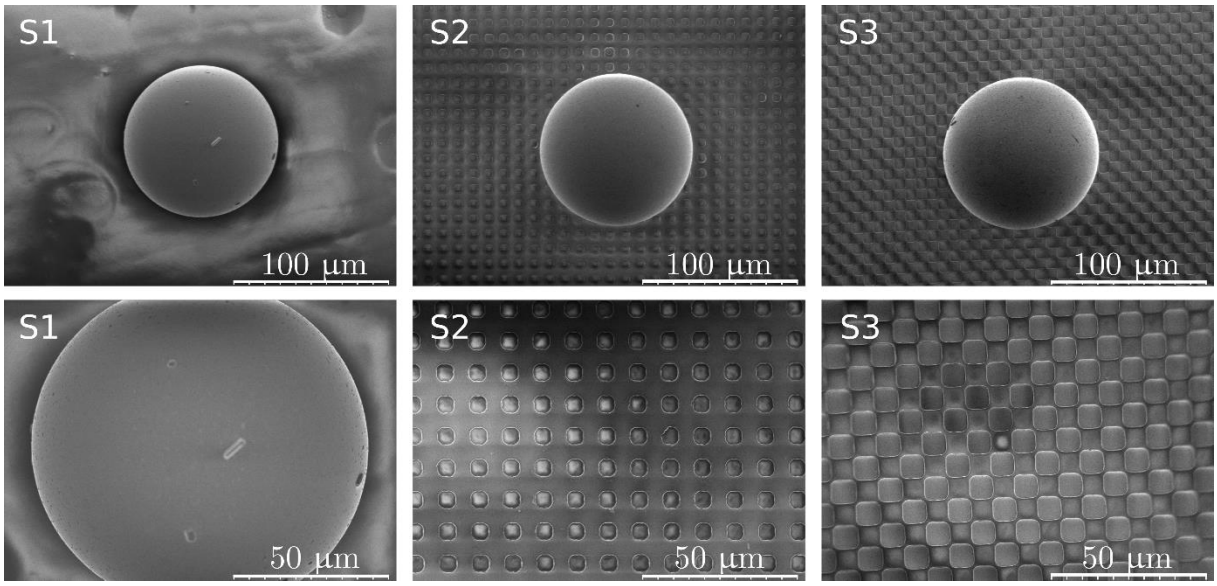

***Fig. 2**: Sample images of particles and three substrates (S1, S2 and S3) taken with a scanning electron microscope (SEM) at two different magnifications. Color gradients in the micrographs are caused by charging effects of the insulating samples during SEM image acquisition*.

2.4. Force measurement with Atomic Force Microscopy

To measure the adhesion force distribution between a single particle and the substrates, the following colloidal probe AFM-based procedure is used. A Park Systems NX12 atomic force

microscope is utilized for colloidal probe preparation, cantilever characterization, which includes calibration, and force-distance measurements. As illustrated in Figure 3, the colloidal probe cantilevers are prepared by gluing a representative 100 µm spherical particle, which involve Ber-Fix UV-Kleber with an All-In-One Aluminum-coated B type cantilever from Budget Sensors (Babel & Rudolph, 2019). Prior to attaching the particle, the force constant of the cantilever is determined using the procedure described in the authors' previous work (Rudolph & Peuker, 2014), which contains all the relevant details about the force constant calibration. Here, along with any other static mode colloidal probe AFM, the force constant is calibrated based on the resonance frequency of the cantilever prior to attaching the particle, which alters the resonance frequency but not the force constant. After hardening of the glue, the colloidal probe cantilever is inspected under the microscope for proper positioning of the particle. Before the first measurement, the AB-sensitivity, that is the relation between signal intensity and bending, is determined with a force-distance contact scan on a Si-wafer substrate. For the adhesion measurements, the substrates are placed under the AFM. A 30 min waiting time allows for equilibration with respect to temperature and adsorption/desorption of gas molecules under the ambient conditions. For each substrate, the force-distance measurements are performed on a square area of 100 x 100 µm^2 with a total of 256 single force-distance measurements measured in triplicates. The adhesion forces are determined from the retrace curves as the absolute maxima. The force limit is kept constant at 220 nN and the z-scanner speed is set to 0.3 µm/s.

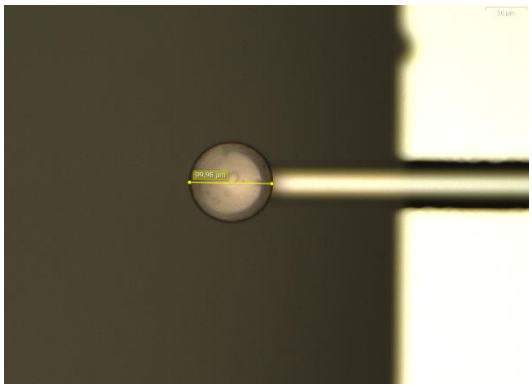

***Fig. 3**: Glass particle attached to cantilever and used for the pull-off force measurements.*

2.5. Particle resuspension in the wind channel

The wind channel is the same as that presented in the authors' previous work (Banari et al., 2021). We hence only recall the most salient features of this experimental set-up. The channel has a length, L = 2 m, and a square cross-section H^2 = 1×1 cm^2, where H is the channel height. A gas flow free of any impurities is created using pressurized clean air. Each substrate is placed 1.5 m downstream of the channel inlet, that is a distance large enough to achieve a fully developed turbulent flow in the measurement section. The presented experiments are performed at room temperature, that is at about T = 15 °C, such that the dynamic viscosity and density of the air are equal to $\mu = 17.89\times10^{-6}$ kg·m^{-1}·s^{-1} and $\rho = 1.225$ kg·m^{-3}, respectively. Prior to experimenting, the inner channel walls are cleaned and dried to ensure an oil- and humidity-free environment that would otherwise adversely affect the resuspension. The flow rate (Q) is varied from zero to Q_{max} = 65 l·min^{-1} with an increment down to 2 l·min^{-1} in areas of high

particle detachment. This corresponds to a maximum air bulk velocity U_{max} = 10.83 m.s^{-1} and a maximum bulk Reynolds number Re_{max} = 7420. The latter is here given by

$$Re = \rho U H / \mu, \tag{1}$$

where $U = Q/H^2$ is the air bulk velocity. Surface functionalization, by allowing a precise control of the wall surface properties, gives rise to exciting opportunities for the fundamental investigation of particle resuspension. With the help of surface functionalization, many limitations associated with the chaotic nature of manually abraded surfaces can be overcome. This work is however a first study and hence we limit ourselves to two roughness types and one particle size. The authors are well aware that a more in-depth parameter study could be performed, for example by further changing the shape of the asperities, their arrangement and the particles. The data presented in this work involve a close collaboration between many laboratories. Coating the wafers, taking the SEM images, measuring the adhesion force distributions and performing the wind channel experiments were done at various places and were quite resource intensive. Manufacturing many coatings is also expensive and will be part of future studies aiming at systematically characterizing the role of wall roughness on resuspension. We hence choose to keep the particle size fixed and, consequently, to focus on the 100-µm glass beads since they are much larger than the typical surface roughness size. In addition, resuspension is here mostly triggered when the equilibrium between aerodynamic and adhesive forces is ruptured because of to the glass beads' size. Resuspension is employed as a rather generic term to describe the particle detachment from a wall surface. The underlying transport mechanisms, that are saltation, rolling, sliding and energy-transfer through particle collisions are not addressed in this study.

To quantify particle resuspension from the three substrates in the wind channel, we employ a conventional procedure widely used in many experimental and numerical studies. First, the particles are manually and sparsely sprinkled over the substrate. The substrate, on which a monolayer bed of particles now lies, is then carefully inserted into the channel test section. A high-resolution camera (MotionPro Y3 HDiablo, Imaging Solutions) equipped with a microscope lens (K2 DistaMax, Infinity Photo-Optical, MX-6 magnification) images a portion of the substrate from the top that is a rectangular field of view with an area set to approximately 2.32 × 1.45 mm^2. A light source (Constellation 120E, Imaging Solutions) illuminates the substrate and the particles from above. Each particle in the image is discretized into about 55 pixels along the diameter. The initial number of particles N_0 in the field of view is determined using semi-automatic procedure. At this stage, the gas in the test section is at rest, that means $Re = 0$. With ImageJ as image processing software (Schneider, Rasband, & Eliceiri, 2012), a Gaussian blur is first employed. An attempt at tagging each individual particle is done by finding the image maxima. The particle tags are then corrected manually. In the presented experiments, the initial particle number N_0 typically varies between about 40 and 200, which corresponds to an initial coverage of the field of view ranging from 9 to 47 % and to surface number concentration ranging from 11 to 60 mm^{-2}, that is the particle number per square millimeters. We note, that the upper bound of the interval, which is only one data set out of thirty, is a bit large in terms of collision frequency compared to the average coverage. Second, the air flow is increased in a stepwise manner. For each value of the flow rate, that is under a constant Reynolds number, the instantaneous particle number $N(Re, t)$ in the field of view rapidly diminishes until it reaches an equilibrium $N(Re, t \to \infty) = N_\infty(Re)$. Our experimental observations show that equilibrium is reached well within seconds. To ensure that equilibrium

is reached under constant Reynolds number, several pictures of the particle bed are taken at regular time intervals. The remaining particle fraction, defined in the field of view as the number of remaining particles at equilibrium divided by that initially obtained at $Re = 0$, is given by

$$f_r = N_\infty(Re)\,/N_0. \tag{2}$$

The specific Reynolds number ($Re_{0.5}$) for which, f_r = 0.5, is defined as the threshold and indicates the critical value at which half of the particles resuspend. The thresholds associated with the bulk velocity ($U_{0.5}$) and the friction velocity ($u^*_{0.5}$) are defined in a similar way. The link between U and u^* is later explained.

3. Results and discussions

3.1. Adhesion force distributions

The measured adhesion forces obtained for the three substrates are shown in Figure 4a in the form of cumulative frequencies. The median adhesion forces between a single particle and the substrates S1, S2 and S3 equate F_a = 168 nN, 82 nN and 197 nN respectively. The median value corresponds here to the 50th percentile (q_{50}) in Figure 4, that is the force abscissa at which each curve crosses the 50% cumulative frequency. These measured adhesion forces agree quantitatively well with previous experimental data found in the literature. Using the centrifugal technique, Salazar-Banda, Felicetti, Goncalves, Coury, and Aguiar (2007) measured the mean adhesion force between a steel surface and phosphatic rock particles with diameters ranging from 20 to 50 µm. Their particles were not spherical and the root-mean-square (rms) roughness of the substrate ranged from 20 to 50 nm. In the present context, the surface of their substrate can be considered smooth. They reported mean adhesion forces between 110 to 330 nN.

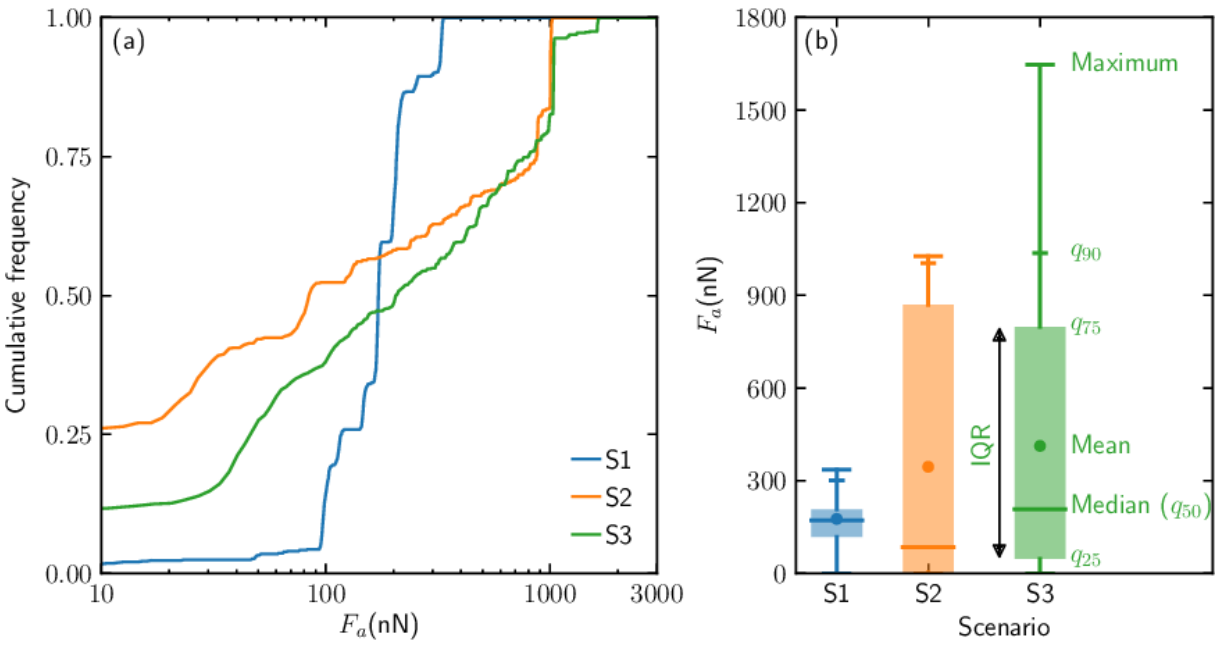

***Fig. 4**: Cumulative frequencies (a) and box plot representations (b) of the adhesion forces F_a measured between a single glass particle and the substrates S1, S2 and S3. q_{25}, q_{75} and q_{90} are the 25th, 75th and 90th percentiles, respectively, $IQR = q_{75} - q_{25}$ the interquartile range.*

The order of magnitude of the median adhesion force is the same for all substrates. Functionalization of the substrates S2 and S3 with microasperities mostly results in a wider and more multimodal distribution. The AFM measurements are performed with no gas flow.

Using AFM, Yang, Zhang, and Hsu (2007) measured the adhesion force between a silicon wafer and spherical glass beads with diameters ranging from 6 to 35 µm. In their work, the substrate roughness was similar to that of our 'smooth' reference substrate S1, that is a few nanometers in amplitude. In all scenarios, they determined mean adhesion forces ranging from 30 to 110 nN. They also reported, that the adhesion forces did not correlate with the bead diameter. Tormoen, Drelich, and Nalaskowski (2005) also performed adhesion force measurements with AFM. The substrate was a silicon wafer and the particles were glass beads with diameters ranging from 10 to 40 µm. They used a first smooth silicon wafer with first-order roughness below 1 nm and a second one, that was artificially roughened with a regular array of triangular microridges with a periodic spacing set to 3 µm and a height to 2 µm. Their measured mean adhesion forces varied between 10 and 110 nN. Interestingly, they also reported that the triangular microridges gave rise to a larger force scattering often exhibiting a multimodal distribution, as opposed to the unimodal distribution associated with their smooth substrate. In their work, the presence of microasperities did not necessarily mean a lower mean adhesion force. We draw here similar conclusions in terms of median value and scattering. The median adhesion forces determined for our three substrates are relatively close to one another. The cumulative frequency associated with the smooth substrate S1 (black curve) exhibits a relatively sharp gradient, indicating a narrower force distribution as opposed to S2 and S3. A common parameter providing information about the scattering is the interquartile range (IQR) illustrated in Figure 4b, which corresponds to the difference between the 75th (q_{75}) and the 25th percentile (q_{25}). The IQR for S2, respectively S3, equals 844 nN, respectively 743 nN. These representative scattering values are much larger than the one associated with S1, which has an IQR equal to 87 nN. The box plot in Figure 4b further illustrates the larger adhesion force scattering in S2 and S3. The 90th percentile (q_{90}) associated with S2 and S3 is about three times as high as that associated with reference S1. The percentile q_{90} equals 301, 1004 and 1037 nN for S1, S2 and S3. The tick position of the 90th percentile relative to the maximum in Figure 4b also gives indication about the likelihood of finding particle strongly adhering particles, which may act as clustering seeds (see section 3.2). Further statistical values, such as the mean and maximum values, are shown in Figure 4b.

3.2. Particle remaining fractions

The results from thirty experiments performed in the wind channel are now presented. For each substrate, ten experiments are carried out. All raw data are available (Gregory. Lecrivain, 2023). First, a selected image sample (see Figure 5) showing an initial particle bed and its subsequent equilibrium states obtained under constant Reynolds numbers is discussed. The sample is shown for increasing Reynolds numbers set to Re = 0, 1711, 2510 and 2738. The remaining fraction associated with each image is also given. The top left panel in Figure 5 further confirms that the initial particle deposit is a monolayer bed. We also note that the particles forming the initial bed are never evenly spread on the surface. As expected, the remaining fraction, which equates unity at $Re = 0$, decreases with increasing Reynolds number. When resuspension starts, striking particle re-arrangement within the bed occurs. We observe the formation of particle islands, hereafter referred to as clusters, on the surface of all three substrates. Cluster formation is well distinguishable in Figure 5, top right. The measured scattering in the adhesion

force helps us explain cluster formation. Some particles adhere more strongly than others to the substrate and only detach at higher wind speed. Such strongly adhering particles hence act as clustering seeds. Other downstream particles, which are loosely attached, roll and eventually come to a halt by colliding with a seed particle. As the cluster grows under constant Reynolds number, particle detachment is further impaired by the lower drag and lift forces induced by flow shielding of neighboring particles (Derksen & Larsen, 2011). On some occasions, we even observed remaining fractions slightly overshooting unity. This occurs because the number of downstream particles accumulating near a seed particle may exceed those carried away from the camera's field of view.

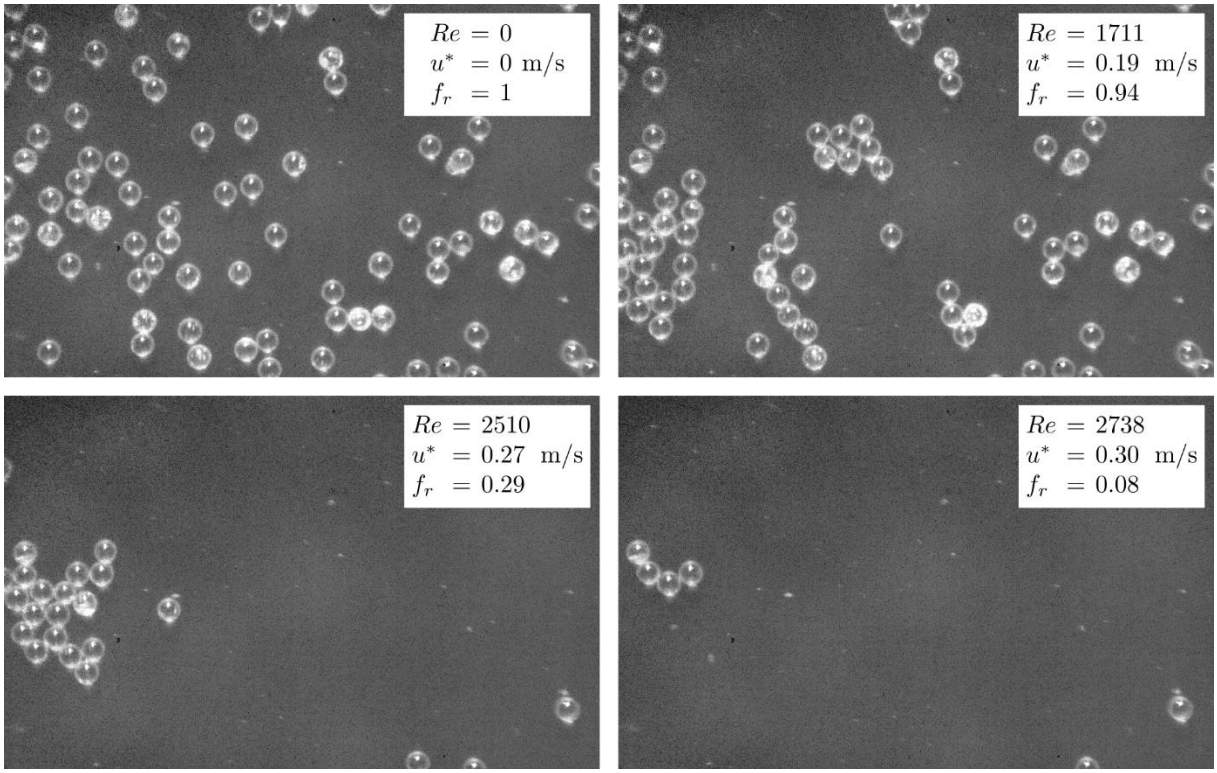

***Fig. 5**: Monolayer bed of particles in equilibrium obtained under constant Reynolds number (Re). The remaining fraction f_r decreases with increasing Reynolds number. The term u^* is the corresponding friction velocity. The camera images were obtained with the rough substrate S2.*

Figure 6 shows the obtained remaining fractions $f_r(Re)$ for the smooth reference substrate S1 (blue circles) and the rough substrates S2 (orange squares) and S3 (green diamonds). For comparison purposes, the data obtained with S2 and S3 are overlaid with the reference blue points.

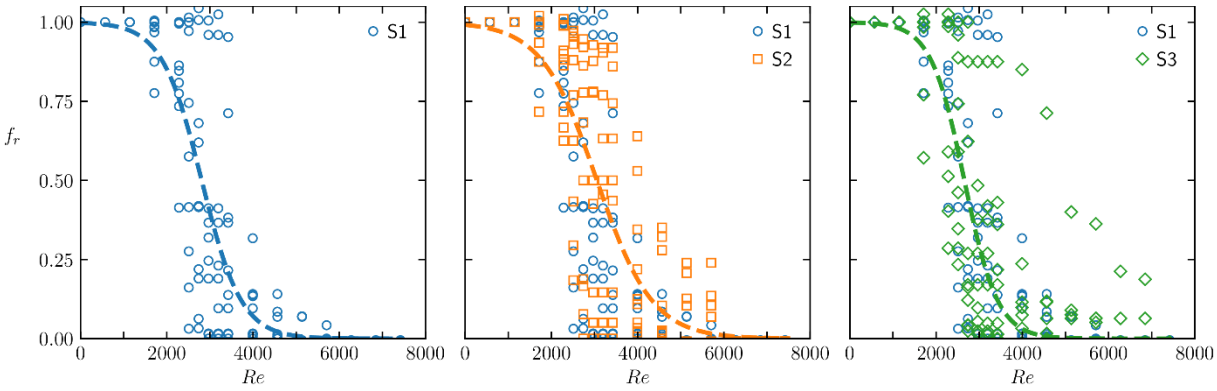

***Fig. 6**: Fraction of particles remaining in the field of view (f_r) against Reynolds number (Re) for the three substrates S1 (blue circles), S2 (orange squares) and S3 (green diamonds). The dashed lines are best-fitted to the experimental data with a hyperbolic tangent function.*

In Figure 6, the experimental points associated with each scenario are determined from ten independent experimental runs. No selection from the raw data has been done. Overall, the resuspension data obtained in the wind channel show a relatively good reproducibility. Irrespective of the substrate, the remaining fractions starts to decrease a $Re \approx 2000$. Beyond $Re > 8000$, all particles have left the camera field of view. The previously mentioned overshooting behavior with punctual values of the remaining fraction greater than unity are also seen in Figure 6.

To determine the threshold Reynolds number $Re_{0.5}$, the experimental data are fitted with a smooth hyperbolic tangent function of the form

$$f_r(Re) = \frac{1}{2}\left[1 - \tanh\left(\frac{Re - Re_{0.5}}{\Delta Re}\right)\right]. \quad (3)$$

The above formulation, which has been suggested by Barth et al. (2014), has advantages. First, the threshold $Re_{0.5}$ is directly included in the function. Second, the denominator ΔRe in Equation (3) relates to the slope of the curve at the ordinate position $f_r = 0.5$. It hence provides a good indication about the scattering, that is the velocity range over which resuspension occurs. In the limit $\Delta Re \to 0$, f_r converges to the step function and resuspension becomes a sudden process similar to that described in Shao and Lu (2000) for wind erosion and would be, in essence, much reminiscent of the Shields theory frequently used for sediment erosion in watery flows (Paphitis, 2001). We find that, with the substrates S1, S2 and S3, half of the particles resuspend at a threshold Reynolds number $Re_{0.5}$ = 2809, 3055 and 2657, respectively. The equivalent threshold velocities are $U_{0.5}$ = 4.10, 4.46 and 3.88 m·s^{-1}. These three thresholds are close to one another, which is consistent with our median adhesion force measurements. We also find ΔRe = 925, 1285 and 777, which respectively converts to velocity denominators ΔU = 1.35, 1.88 and 1.13 m·s^{-1}. These three measures of the scattering are also relatively close to one another. A closer look at Figure 6, especially in the region $Re > 5000$, shows however a higher frequency of nonzero remaining fractions for the rough substrates S2 and S3 compared to the smooth substrate S1. In fact, with the exception of only a few experimental points, all particles are already resuspended from the smooth surface S1 in this upper Reynolds number region. This trend can be related to the higher probability of finding particles with large adhesion forces in S2 and S3. In Figure 4b, the corresponding 75th percentiles are about three

times as large as the maximum adhesion force measured for the smooth substrate S1. Such strongly adhering particles are potential candidates acting as seed particles, trapping other particles colliding with them on the surface and triggering cluster formation as shown in Figure 5. In addition, the IQRs in S2 and S3 are also larger than in S1. This leads to a higher variability in the remaining fractions. See, for instance, the larger spread of green points at fixed Reynolds numbers in Figure 6. We hence can relate particle resuspension at high Reynolds number to the tail of the adhesion force distribution, for which the 75th and 90th percentiles are representative. This confirms our former idea (Henry & Minier, 2018), that statistical information related to the adhesion forces should ideally contain more than the average and the standard deviation for an accurate prediction of the resuspension fraction. Here, our measured adhesion force distributions are clearly not Gaussian but multimodal.

3.3. Comparisons of the threshold velocity with literature data

For comparison purposes, the hyperbolic fits are also shown with selected experimental data taken from other sources. In the aerosol community, the remaining fraction is commonly plotted as a function of the friction velocity (u^*) calculated at the wall. To estimate it, an empirical correlation with an accuracy of about 5 % under fully developed turbulence is presently used (Hartnett, Koh, & McComas, 1962; Jones, 1976). By defining the friction factor as $f = 8(u^*/U)^2$, we solve the modified Kármán–Prandtl equation given by

$$\frac{1}{\sqrt{f}} = 2\log_{10}\left(\beta Re\sqrt{f}\right) - 0.8, \tag{4}$$

where β = 1.125 is a correction coefficient introduced to account for the square cross-section of the channel. We are well aware, that Equation (4) is only valid for smooth channels and $Re > 4300$. Present experimental observations show that resuspension mostly occurs for Reynolds number ranging from 2000 to 6000. Favoring a continuous function linking the Reynolds number to the friction velocity, the formulation applicable to the laminar and intermediate regimes is here left out. Using Equation (4) outside its range of validity does not change the following analysis. Authors interested in using our data, for instance to validate their model, are encouraged to use the Reynolds number. Figure 7 compares our results to literature data. Barth et al. (2014) used 20-µm glass spheres and a steel plate with sub-micrometer roughness, Reeks and Hall (2001) 10-µm alumina spheres (labeled as 2001a), 20-µm alumina spheres (labeled as 2001b) and a polished stainless-steel substrate, Del Bello et al. (2018) ash particles with diameter ranging from 125 to 250 µm and a substrate with wall roughness in the same order as the particle size. The above data are charted in Figure 7 with a logarithmic scale on the abscissa for better illustration. The remaining fractions obtained with the present smooth and rough substrates compare well with those from other studies. In Figure 7, the threshold velocity ($u^*_{0.5}$) determined by other authors varies between 0.2 m.s^{-1} to 0.6 m.s^{-1}. The present threshold velocities are equal to 0.30, 0.32 and 0.28 m·s^{-1} for S1, S2 and S3.

3.4. Potential limitations of this study

This study slightly differs from others. In Barth et al. (2014), the substrates from which the spherical particles resuspended, were made of steel. The Young's modulus of steel is much greater than that of the functionalized coating, here made of resin (see section 2.3). The roughness asperities likely deform, which might make it difficult to estimate the number contacts between a particle and the rough substrate. The spheres exhibit some roughness too.

In addition, individual damaged asperities were also observed with every experiment. We hence limited the number of runs per substrate in the wind channel to ten. The adhesion force is dependent on the ambient atmospheric conditions. Despite doing our best minimize these adverse effects, the measurements with the AFM and in the wind channel were performed separately and had to be made at different times and locations. Finally, the AFM measurements are done on a rather small surface, typically in the order of 10^{-2} mm^2. The remaining fractions are rather integral values obtained from a much larger wall surface, typically a few square millimeters (mm^2).

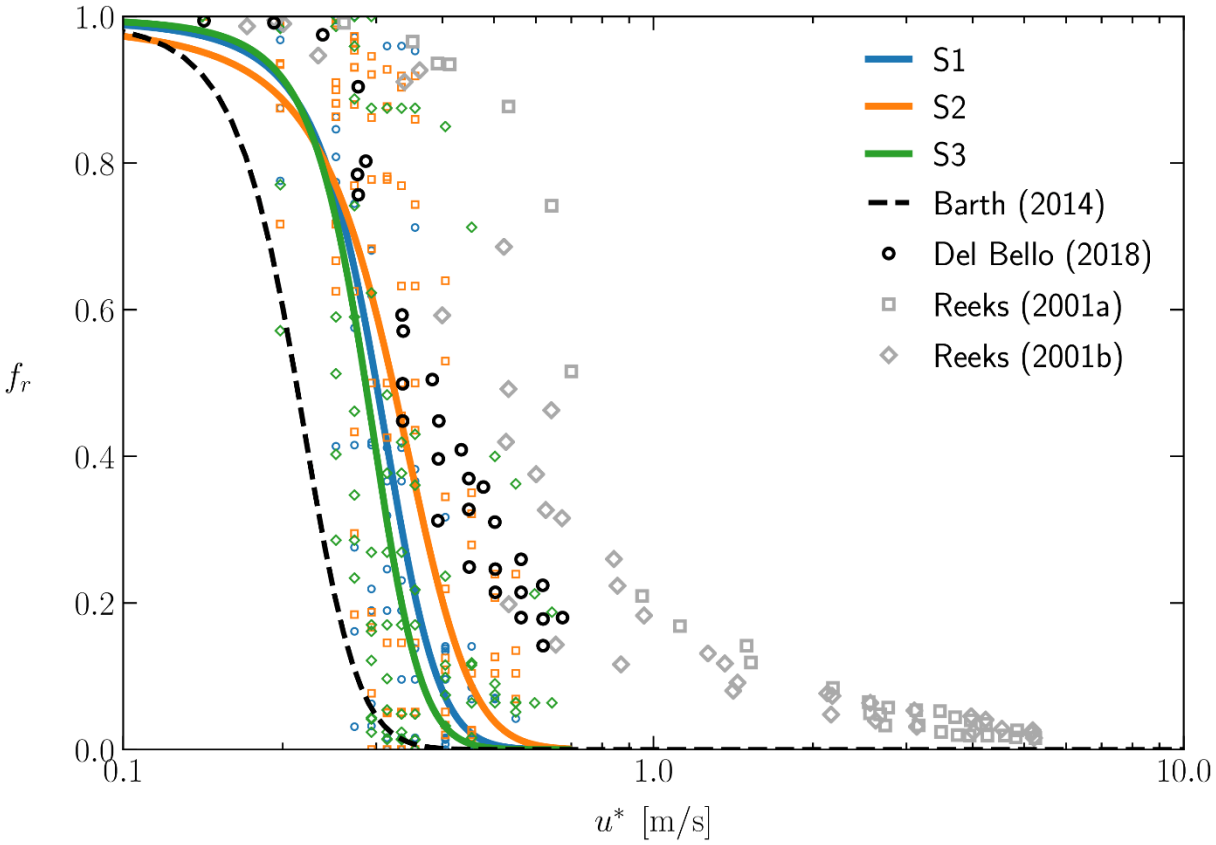

***Fig. 7**: Comparison of the fraction of remaining particles (f_r) against the friction velocity (u^*) with literature data.*

Conclusions

The resuspension of glass particles with a 100-µm diameter exposed to a turbulent gas flow was studied at Reynolds number up to 8000. Our measurements include adhesion force and remaining fractions against increasing gas velocity. Three substrates were used, namely a smooth and two artificially roughened ones. Three main messages emerge from our study and further stress the importance of using well-defined asperities rather than a manually abraded surface.

- The chaotic nature of a manually abraded surfaces, in terms of highly heterogenous asperity size, shape and spatial distribution, is responsible for the lack of correlation between surface roughness and threshold velocity. To highlight this, we briefly recall previous experimental results (Barth et al., 2014; Jiang et al., 2008). In those works, steel substrates with increasing wall roughness were used. The curves $f_r(u^*)$ did not necessarily lead to the conclusion that

an increase in wall roughness was associated with a lower threshold velocity $u_{0.5}^{*}$. With identical spherical beads, the threshold velocities were often close to one another irrespective of the wall roughness and in some cases, an increase in the threshold velocity was even reported for higher roughness.

- Our results obtained with functionalized wall surfaces, that are roughened with well-defined microasperities, do behave as expected (Audry, Ramos, & Charlaix, 2009; Tormoen et al., 2005). Compared to the reference scenario S1 exhibiting a roughness profile in the nanoscale, the microasperities in S2 and S3 lead to a larger scattering in the adhesion forces and the friction velocities. How the adhesion force distribution relates to surface roughness depends on the particle diameter, the roughness size along with the deformability of the particle and substrate, as this determines the number of asperities in contact with the particle.
- Our measurements of the adhesion force distribution and resuspension fraction as a function of the Reynolds number can be used for future model development and validation. Our experiments are motivated by theories of contact mechanics and state-of-the-art simulations modelling asperities as spherical caps (Guingo & Minier, 2008; Henry & Minier, 2014b). In this context, we have experimentally explored particle resuspension from wall surfaces functionalized with well-defined roughness elements, which could be used in simulations.

Acknowledgements

This work was funded by the Helmholtz Associations Initiative and Networking Fund within the frames of the Helmholtz Climate Initiative (HI-CAM), the Helmholtz project CORAERO and the Helmholtz Innovation Lab, Clean Water Technology (CLEWATEC). Funding by the European Social Fund and the Free State of Saxony (Grant Number 100284305) is also acknowledged.

Author contributions

A.B. and G.L. conceptualized and designed the study. A.B., G.L. and E.M. performed the wind channel experiments. K.G. and M.R. performed the adhesion force measurements. P.L. and K.Z. prepared the substrates by functionalizing their surfaces. R.H. performed the SEM image analysis of the substrates and particles. C.H. made a significant contribution to the discussions. C.H., M.B. and U.H. aided in interpreting the results. G.L. and U.H. contributed to the acquisition of the financial support for this work. All authors discussed the results and reviewed the manuscript.

Data availability

All raw data used in this work have been made available with a DOI number (Gregory. Lecrivain, 2023).

Highlights

- Surface functionalization is used to fabricate wall surfaces with well-defined asperities represented by cylindrical micropillars and microcubes.

- The resuspension of glass particles with a 100-µm diameter exposed to a turbulent gas flow was studied at Reynolds number up to 8000.
- The response of the manufactured surfaces in relation to adhesion force distribution and threshold friction velocity, at which 50 % of the particles resuspend, is examined.
- The well-defined microasperities have little to moderate effect on the median adhesion force and the threshold velocity. The data scattering is however much more affected.

References

Adebiyi, A., Kok, J. F., Murray, B. J., Ryder, C. L., Stuut, J.-B. W., Kahn, R. A., . . . Meng, J. (2023). A review of coarse mineral dust in the Earth system. *Aeolian Research, 60*. doi:10.1016/j.aeolia.2022.100849

Amato-Lourenco, L. F., Dos Santos Galvao, L., de Weger, L. A., Hiemstra, P. S., Vijver, M. G., & Mauad, T. (2020). An emerging class of air pollutants: Potential effects of microplastics to respiratory human health? *Science of the Total Environment, 749*, 141676. doi:10.1016/j.scitotenv.2020.141676

Audry, M. C., Ramos, S., & Charlaix, E. (2009). Adhesion between highly rough alumina surfaces: an atomic force microscope study. *J Colloid Interface Sci, 331*(2), 371-378. doi:10.1016/j.jcis.2008.11.050

Babel, B., & Rudolph, M. (2019). Fast preparation and recycling method for colloidal probe cantilevers in hydrophobic mapping applications. *MethodsX, 6*, 651-659. doi:10.1016/j.mex.2019.03.010

Banari, A., Henry, C., Eidt, R. H. F., Lorenz, P., Zimmer, K., Hampel, U., & Lecrivain, G. (2021). Evidence of collision-induced resuspension of microscopic particles from a monolayer deposit. *Physical Review Fluids, 6*(8). doi:10.1103/PhysRevFluids.6.L082301

Banari, A., Hertel, D., Schlink, U., Hampel, U., & Lecrivain, G. (2023). Simulation of particle resuspension by wind in an urban system. *Environmental Fluid Mechanics, 23*(1), 41-63. doi:10.1007/s10652-022-09905-x

Barth, T., Preuß, J., Müller, G., & Hampel, U. (2014). Single particle resuspension experiments in turbulent channel flows. *Journal of Aerosol Science, 71*, 40-51. doi:10.1016/j.jaerosci.2014.01.006

Bourouiba, L. (2021). The fluid dynamics of disease transmission. *Annual Review of Fluid Mechanics, 53*(1), 473-508. doi:10.1146/annurev-fluid-060220-113712

Brambilla, S., & Brown, M. J. (2020). Impact of the adhesion-force lever-arm "a" on the Rock 'n' Roll resuspension model and how to compute it from contact mechanics. *Journal of Aerosol Science, 143*. doi:10.1016/j.jaerosci.2020.105525

Brambilla, S., Speckart, S., & Brown, M. J. (2017). Adhesion and aerodynamic forces for the resuspension of non-spherical particles in outdoor environments. *Journal of Aerosol Science, 112*, 52-67. doi:10.1016/j.jaerosci.2017.07.006

Brambilla, S., Speckart, S., Rush, M. N., Montano, G. A., & Brown, M. J. (2018). Glass particle resuspension from a contaminated (dirty) glass surface. *Journal of Aerosol Science, 123*, 122-130. doi:10.1016/j.jaerosci.2018.06.011

Cho, M.-C., Jo, Y.-G., Son, J. A., Kim, I., Oh, C., & Yook, S.-J. (2021). Deposition characteristics of soot and tire-wear particles on urban tree leaves. *Journal of Aerosol Science, 155*. doi:10.1016/j.jaerosci.2021.105768

Ciavarella, M., Joe, J., Papangelo, A., & Barber, J. R. (2019). The role of adhesion in contact mechanics. *Journal of the Royal Society Interface, 16*(151), 20180738. doi:10.1098/rsif.2018.0738

Cui, Y., & Sommerfeld, M. (2022). Lattice-Boltzmann simulations for analysing the detachment of micron-sized spherical particles from surfaces with large-scale roughness structures. *Particuology, 61*, 47-59. doi:10.1016/j.partic.2021.05.004

Del Bello, E., Taddeucci, J., Merrison, J. P., Alois, S., Iversen, J. J., & Scarlato, P. (2018). Experimental simulations of volcanic ash resuspension by wind under the effects of atmospheric humidity. *Scientific Reports, 8*(1), 14509. doi:10.1038/s41598-018-32807-2

Derksen, J. J., & Larsen, R. A. (2011). Drag and lift forces on random assemblies of wall-attached spheres in low-Reynolds-number shear flow. *Journal of Fluid Mechanics, 673*, 548-573. doi:10.1017/s0022112010006403

Fuller, K. N. G., & Tabor, D. (1997). The effect of surface roughness on the adhesion of elastic solids. *Proceedings of the Royal Society of London. A. Mathematical and Physical Sciences, 345*(1642), 327-342. doi:10.1098/rspa.1975.0138

Goldasteh, I., Ahmadi, G., & Ferro, A. R. (2013). Wind tunnel study and numerical simulation of dust particle resuspension from indoor surfaces in turbulent flows. *Journal of Adhesion Science and Technology, 27*(14), 1563-1579. doi:10.1080/01694243.2012.747729

Guingo, M., & Minier, J.-P. (2008). A new model for the simulation of particle resuspension by turbulent flows based on a stochastic description of wall roughness and adhesion forces. *Journal of Aerosol Science, 39*(11), 957-973. doi:10.1016/j.jaerosci.2008.06.007

Hartnett, J. P., Koh, J. C. Y., & McComas, S. T. (1962). A Comparison of Predicted and Measured Friction Factors for Turbulent Flow Through Rectangular Ducts. *Journal of Heat Transfer, 84*(1), 82-88. doi:10.1115/1.3684299

Henry, C., & Minier, J.-P. (2014a). Progress in particle resuspension from rough surfaces by turbulent flows. *Progress in Energy and Combustion Science, 45*, 1-53. doi:10.1016/j.pecs.2014.06.001

Henry, C., & Minier, J.-P. (2014b). A stochastic approach for the simulation of particle resuspension from rough substrates: Model and numerical implementation. *Journal of Aerosol Science, 77*, 168-192. doi:10.1016/j.jaerosci.2014.08.005

Henry, C., & Minier, J.-P. (2018). Colloidal particle resuspension: On the need for refined characterisation of surface roughness. *Journal of Aerosol Science, 118*, 1-13. doi:10.1016/j.jaerosci.2018.01.005

Henry, C., Minier, J.-P., & Brambilla, S. (2023). Particle resuspension: Challenges and perspectives for future models. *Physics Reports, 1007*, 1-98. doi:10.1016/j.physrep.2022.12.005

Hospodsky, D., Qian, J., Nazaroff, W. W., Yamamoto, N., Bibby, K., Rismani-Yazdi, H., & Peccia, J. (2012). Human occupancy as a source of indoor airborne bacteria. *PLoS One, 7*(4), e34867. doi:10.1371/journal.pone.0034867

Hu, R., Johnson, P. L., & Meneveau, C. (2023). Modeling the resuspension of small inertial particles in turbulent flow over a fractal-like multiscale rough surface. *Physical Review Fluids, 8*(2). doi:10.1103/PhysRevFluids.8.024304

Jiang, Y., Matsusaka, S., Masuda, H., & Qian, Y. (2008). Characterizing the effect of substrate surface roughness on particle–wall interaction with the airflow method. *Powder Technology, 186*(3), 199-205. doi:10.1016/j.powtec.2007.11.041

Jones, O. C. (1976). An improvement in the calculation of turbulent friction in rectangular ducts. *Journal of Fluids Engineering, 98*(2), 173-180. doi:10.1115/1.3448250

Klose, M., & Shao, Y. (2013). Large-eddy simulation of turbulent dust emission. *Aeolian Research, 8*, 49-58. doi:10.1016/j.aeolia.2012.10.010

Lecrivain, G. (2023). Raw data related to publication "Influence of engineered roughness microstructures on adhesion and turbulent resuspension of microparticles" by Banari et al. doi:10.14278/rodare.2426, https://rodare.hzdr.de/record/2426

Lecrivain, G., Vitsas, A., Boudouvis, A. G., & Hampel, U. (2014). Simulation of multilayer particle resuspension in an obstructed channel flow. *Powder Technology, 263*, 142-150. doi:10.1016/j.powtec.2014.05.009

Maji, S., Urakawa, O., & Inoue, T. (2014). Viscoelastic properties and birefringence of phenolic resins. *Polymer journal, 46*(5), 272-276. doi:10.1038/pj.2013.97

Mikellides, I., Chen, N., Liao, S., Droz, E., Strimbu, Z., Stricker, M., . . . Steltzner, A. (2020). Experiments in particle resuspension and transport for the assessment of terrestrial-borne biological contamination of the samples on the mars 2020 mission. *Planetary and Space Science, 181*. doi:10.1016/j.pss.2019.104793

Monk, J. D., Haskins, J. B., Bauschlicher, C. W., & Lawson, J. W. (2015). Molecular dynamics simulations of phenolic resin: Construction of atomistic models. *Polymer, 62*, 39-49. doi:10.1016/j.polymer.2015.02.003

Mukai, C., Siegel, J. A., & Novoselac, A. (2009). Impact of Airflow Characteristics on Particle Resuspension from Indoor Surfaces. *Aerosol Science and Technology, 43*(10), 1022-1032. doi:10.1080/02786820903131073

Nasr, B., Ahmadi, G., Ferro, A. R., & Dhaniyala, S. (2019). A model for particle removal from surfaces with large-scale roughness in turbulent flows. *Aerosol Science and Technology, 54*(3), 291-303. doi:10.1080/02786826.2019.1692126

Paphitis, D. (2001). Sediment movement under unidirectional flows: an assessment of empirical threshold curves. *Coastal Engineering, 43*(3-4), 227-245. doi:10.1016/s0378-3839(01)00015-1

Peillon, S., Autricque, A., Redolfi, M., Stancu, C., Gensdarmes, F., Grisolia, C., & Pluchery, O. (2019). Adhesion of tungsten particles on rough tungsten surfaces using Atomic Force Microscopy. *Journal of Aerosol Science, 137*. doi:10.1016/j.jaerosci.2019.105431

Peillon, S., Gélain, T., Payet, M., Gensdarmes, F., Grisolia, C., & Pluchery, O. (2022). Adhesion forces of radioactive particles measured by the Aerodynamic Method–Validation with Atomic Force Microscopy and comparison with adhesion models. *Journal of Aerosol Science, 165*. doi:10.1016/j.jaerosci.2022.106037

Rabinovich, Y. I., Adler, J. J., Ata, A., Singh, R. K., & Moudgil, B. M. (2000). Adhesion between Nanoscale Rough Surfaces: I. Role of Asperity Geometry. *Journal of the Royal Society Interface, 232*(1), 17-24. doi:10.1006/jcis.2000.7168

Reeks, M. W., & Hall, D. (2001). Kinetic models for particle resuspension in turbulent flows: theory and measurement. *Journal of Aerosol Science, 32*(1), 1-31. doi:10.1016/s0021-8502(00)00063-x

Rudolph, M., & Peuker, U. A. (2014). Mapping hydrophobicity combining AFM and Raman spectroscopy. *Minerals Engineering, 66-68*, 181-190. doi:10.1016/j.mineng.2014.05.010

Salazar-Banda, G. R., Felicetti, M. A., Goncalves, J. A. S., Coury, J. R., & Aguiar, M. L. (2007). Determination of the adhesion force between particles and a flat surface, using the centrifuge technique. *Powder Technology, 173*(2), 107-117. doi:10.1016/j.powtec.2006.12.011

Schneider, C. A., Rasband, W. S., & Eliceiri, K. W. (2012). NIH Image to ImageJ: 25 years of image analysis. *Nat Methods, 9*(7), 671-675. doi:10.1038/nmeth.2089

Shao, Y., & Lu, H. (2000). A simple expression for wind erosion threshold friction velocity. *Journal of Geophysical Research: Atmospheres, 105*(D17), 22437-22443. doi:10.1029/2000jd900304

Shinohara, N., & Yoshida-Ohuchi, H. (2021). Resuspension and deposition of PM2.5 and PM10 containing radiocesium during and after indoor cleaning of uninhabited houses in Fukushima, Japan. *Chemosphere, 272*. doi:10.1016/j.chemosphere.2021.129934

Soltani, M., & Ahmadi, G. (1999). Detachment of rough particles with electrostatic attraction from surfaces in turbulent flows. *Journal of Adhesion Science and Technology, 13*(3), 325-355. doi:10.1163/156856199x00668

Tormoen, G. W., Drelich, J., & Nalaskowski, J. (2005). A distribution of AFM pull-off forces for glass microspheres on a symmetrically structured rough surface. *Journal of Adhesion Science and Technology, 19*(3-5), 215-234. doi:Doi 10.1163/1568561054352621

Visez, N., Ivanovsky, A., Roose, A., Gosselin, S., Sénéchal, H., Poncet, P., & Choël, M. (2019). Atmospheric particulate matter adhesion onto pollen: a review. *Aerobiologia, 36*(1), 49-62. doi:10.1007/s10453-019-09616-9

Yang, S., Zhang, H., & Hsu, S. M. (2007). Correction of random surface roughness on colloidal probes in measuring adhesion. *Langmuir, 23*(3), 1195-1202. doi:10.1021/la0622828

Ziskind, G., Fichman, M., & Gutfinger, C. (1997). Adhesion moment model for estimating particle detachment from a surface. *Journal of Aerosol Science, 28*(4), 623-634. doi:10.1016/s0021-8502(96)00460-0